J Mater Sci (2011) 46:5097–5103
DOI 10.1007/s10853-011-5439-2

Influence of hot working on microstructure and mechanical behavior of high nitrogen stainless steel

Cheng-miao Hong · Jie Shi · Li-yuan Sheng · Wen-quan Cao · Wei-jun Hui · Han Dong

Received: 6 February 2011 / Accepted: 2 March 2011 / Published online: 11 March 2011

Abstract The relationship between microstructures and mechanical properties of a high nitrogen stainless (HNS) steel (0.65N–1.8Ni, wt%) manufactured by argon oxygen decarburization and continuous casting was investigated in this article. The plates with different thicknesses were obtained by thermo-mechanical control process. The results revealed that the plates prepared by hot rolled and solution treated possessed good balanced mechanical properties, i.e., satisfactory strength and higher toughness. Compared with hot-rolled and solution-treated plates, the hot-rolled plate had much higher tensile strength, but its impact toughness was extremely low. Furthermore, with the increase of deformation strain, the plate with finer grains, more precipitates and higher strength was achieved, but its plasticity decreased obviously. The worm-like carbides formed along the grain boundary during the finish rollings at 850 °C, which are detrimental to the toughness of hot-rolled plates. In addition, small amount of ferrite precipitated in the steel due to the non-equilibrium solidification during continuous casting, and to ensure full austenitic structure, composition design method was recommended.

C. Hong (✉) · J. Shi · W. Cao · W. Hui · H. Dong
Institute for Structural Materials, Central Iron and Steel Research Institute, No. 76 Xueyuan Nanlu, Haidian District, Beijing 100081, People's Republic of China
e-mail: peterhong79@yahoo.cn

L. Sheng
Shenzhen Institute, Peking University, Shenzhen 518057, China

Introduction

Nitrogen-alloyed austenitic stainless steels are becoming an increasing important new class of engineering materials, because they can satisfy these requirements, such as high strength, ductility, good toughness, and resistance to localized corrosion [1–3]. It is established that such high performance result from nitrogen in solid solution. The high austenitizing capacity of nitrogen makes it possible to reduce the expensive nickel, which offers additional advantage of cost-saving. The nitrogen in solution increases not only the strength and toughness, but also largely the internal friction which results in enormously high stain rate sensitivity. These properties make nitrogen-alloyed austenitic steels a potential candidate as an armor steel [4–7]. The solubility of nitrogen increases with increasing manganese and chromium contents, therefore nitrogen alloying could be effectively applied in the alloy system of Cr–Mn or Cr–Mn–Ni [8, 9].

The alloying composition and processing adopted can greatly influence the microstructure and hence ultimately determine the mechanical properties of theses austenitic stainless steels. Different processing conditions can bring diverse microstructural characteristics, which can lead to versatile properties [10, 11]. So understanding the microstructure is very important to achieve optimal properties for the steels.

The purpose of this study is to study the relationship between microstructures and mechanical properties of a low nickel austenitic stainless steel alloyed with 0.65N (wt%) fabricated by hot rolling and subsequent solution treatment (ST). The experimental results and analysis provided by this article will assist in composition design and mechanical processing optimization for this kind of alloys.

Experimental

The material used for this study was a nitrogen-alloyed austenitic stainless steel produced by Taiyuan Iron and Steel Co. Ltd., and the manufacturing route was: 40 t Electric Arc Furnace (EAF) → 40 t Argon Oxygen Decarburization (AOD) → 40 t Ladle Furnace (LF) → continuous casting → 180 mm (thickness) × 1010 mm (width) slab. The nominal chemical composition (wt%) of the as-received slab is 0.11C, 21.4Cr, 15.8Mn, 1.8Ni, 0.65N, and balance Fe. The slab was reheated to 1250 °C for 2 h and hot rolled (HR) to attain plates with different thickness of 10 mm (HR1), 14 mm and 20 mm (HR2), and after finish rolling at about 850 °C the steels were directly water quenched. ST was carried out on the plate of 14 mm (indicated as HRST14 hereinafter) at 1080 °C for 1 h.

Mechanical properties of the plates were assessed by room temperature tensile and −40 °C impact test with standard Charpy V-notch specimens. All these samples were cut along the transverse direction of the plates, and average value was obtained through several specimens for the sake of data accuracy.

In order to make the grain morphology especially the grain boundaries clear, specimens were aged at 650 °C for 1 h, during which grain boundary carbides and nitrides will precipitate while the grain size does not change. The samples for microstructure observation were mechanically ground and electrolytically etched in a solution of 10% chromiumtrioxide and H_2O. The microstructure observation was carried out on an optical microscope (OM). Chemical extraction was used to analyze the amount and types of the precipitates formed during hot rolling. First, the specimen was decomposed in a solution of 1% tetramethyl ammonium chloride and 10% acetylacetone methanol, with the current density $I = 0.08$–0.10 A/cm^2, $T = -5$ to -10 °C, then the extracted particles were collected by filtering film with apertures of 0.2 μm. Finally, structural characteristics of the particles were investigated by using an XPertPRO MPO X-ray diffractometer. In addition, transmission electron microscopy (TEM) and scanning electron microscopy (SEM) were also applied to investigate the morphology of precipitates, orientation with the matrix, fractography of the impact samples and fracture mechanism also discussed.

Results and discussion

Microstructural characteristics

Optical microscopy

Figure 1 shows the grain morphology of high nitrogen stainless (HNS) under different processing conditions.

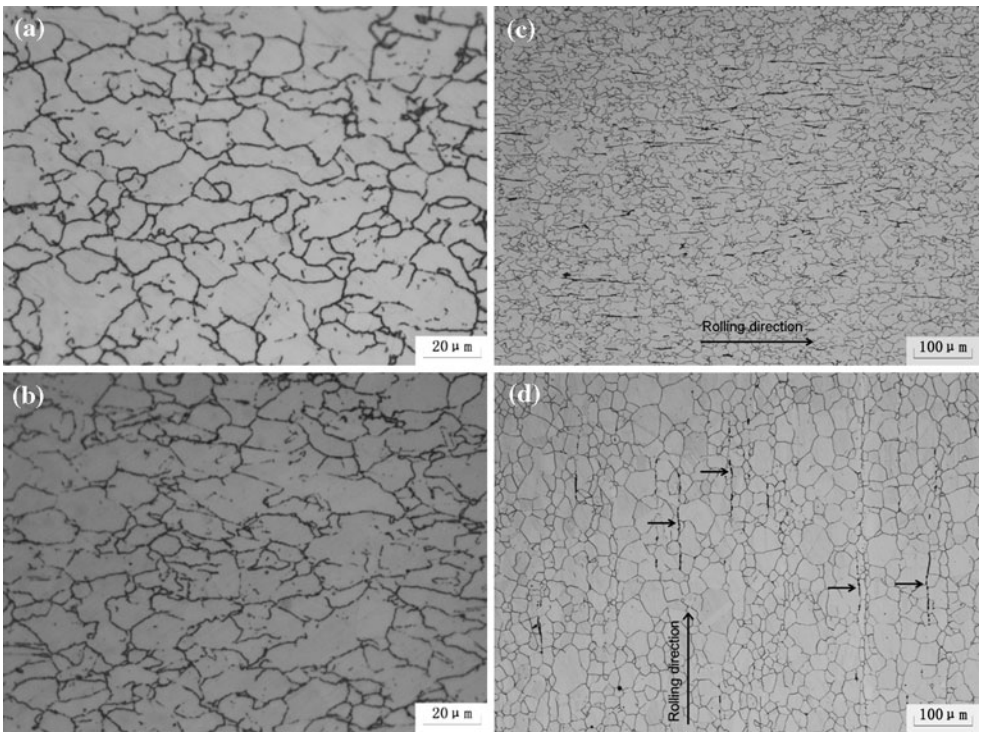

Fig. 1 Grain morphology of HNS under different processing conditions (aged at 650 °C for 1 h) **a** HR2; **b** HR1, elongated austenitic grains; **c** HR2, ferrites distributed in the center region of the plate along the longitudinal direction; and **d** HRST14, equiaxed grains and trace amount of ferrite

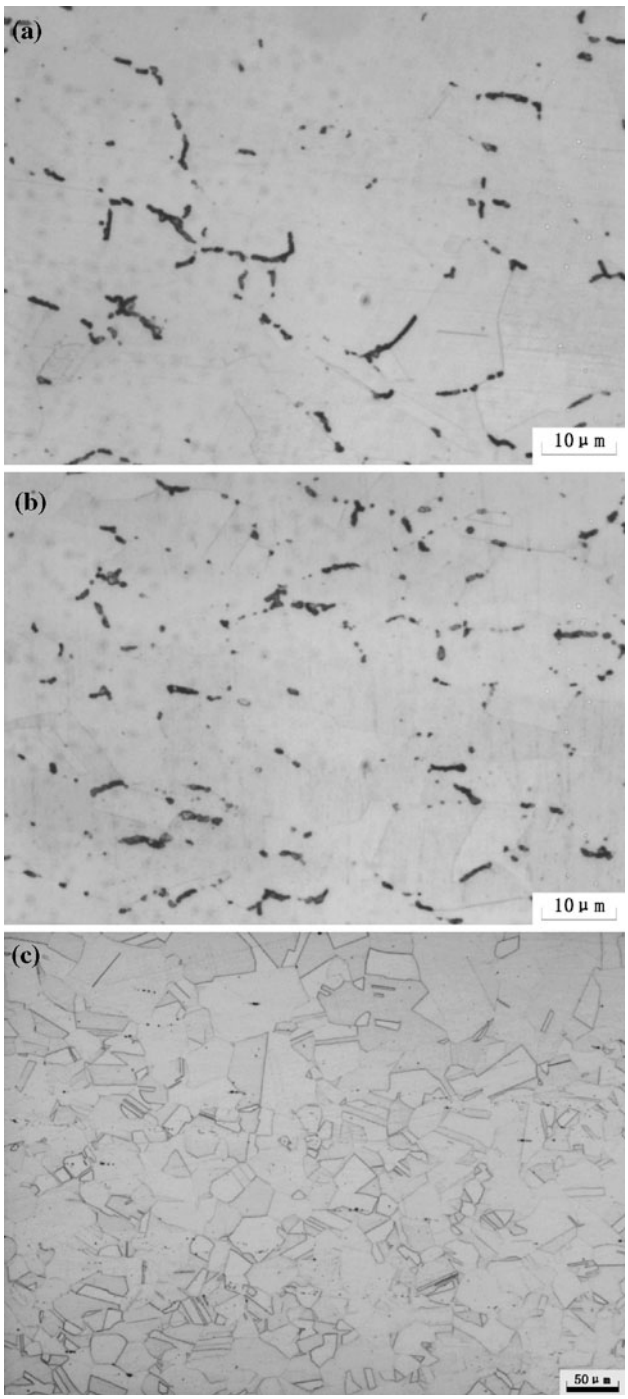

Fig. 2 Optical microstructure of the as-received plates **a** HR2, warm-like precipitates along grain boundary; **b** HR1, finer precipitates and distribute more uniformly; and **c** HRST14, annealing twins and no precipitates

The hot-rolled plate exhibits a deformed structure with elongated austenitic grains in the direction of hot rolling, and this is because the final processing passes have entered the no-recrystallization region, with average grain sizes of 9.84 and 11.37 μm, respectively, as shown in Fig. 1a and b. There is also a small amount of ferrites mainly distributed in the center region of the plate along the longitudinal direction, as shown in Fig. 1c, and its existence will be discussed in the following part. After ST the microstructure consists of equiaxed grains of about 18.68 μm, compared with the hot-rolled ones and its ferrite quantity is obviously less which is due to the dissolution during the process of ST.

Grain boundary and lamellar precipitates were observed in both hot-rolled plates (Fig. 2a, b), however, their morphology and distribution are different. The precipitates in HR1 are a little finer, and distribute uniformly along the grain boundary. As for the HR2 plate, the size of warm-like precipitates even reaches 7 μm. The main difference of hot-rolling process for these two plates is that the rolling passes are increased for the 10 mm plate which means higher strain at final stage. The increased strain at lower temperatures is in favor of precipitate refinement. When hot rolling is followed by ST at 1080 °C for 1 h and subsequently direct quenching in water, the microstructure contains a large amount of annealing twins and the precipitates disappear, as shown in Fig. 2c.

Precipitate characteristics

Figure 3 shows the results of X-ray diffraction studies on the extracted particles from hot-rolled plates, and the characteristics analysis of precipitates is presented in Table 1. It can be seen that only $M_{23}C_6$ can be detected in the HR2 plate. With the increase of deformation, more carbides precipitate from the matrix, and trace amount of nitride-$(CrFe)_2N_{1-X}$ appears. The ratio of C/N will determine the precipitation types. In some literatures [12–14] only nitrides were reported, because of their lower C/N (less than 0.09). For the steel used in this study the value of C/N is 0.17, so carbides $M_{23}C_6$ are its main precipitates.

The bright field TEM micrographs of the hot-rolled plate are shown in Fig. 4. It is clear that the high deformation has led to high-density dislocations in the matrix, especially along grain boundaries. The dislocations tangle with each other inside of grains and some form into network. In addition, carbides in the shape of long bars along the grain boundaries are observed. The selected area electron diffraction (SAED) pattern of the carbide precipitates is shown in Fig. 4b. From the image, it can be determined that the carbide is $M_{23}C_6$. Moreover, from the SAED pattern it can be found that the carbide precipitate has the orientation relationship with the matrix as $[110]_\gamma//[110]_{M23C6}$. Furthermore, the fringe spots of the SAED pattern have a tendency to elongation, so it can be concluded that great stress still exist in the matrix.

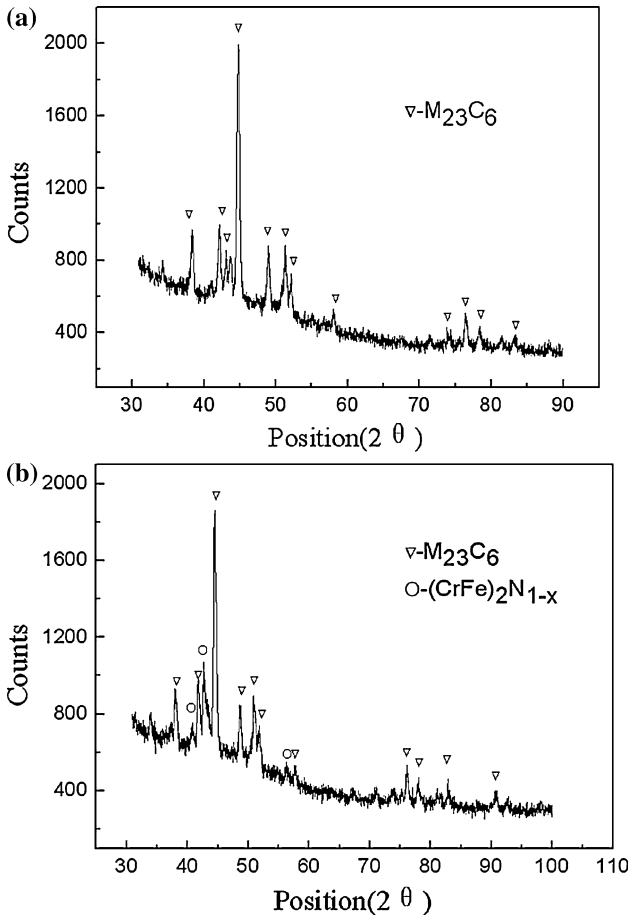

Fig. 3 X-ray diffraction patterns of hot-rolled HNS **a** HR2 and **b** HR1, $(CrFe)_2N_{1-X}$ appears

Mechanical properties

The mechanical properties (average value) of high nitrogen steel with different processing conditions are given in Table 2. It can be seen that the mechanical resistance, represented by yield strength ($R_{p0.2}$) and ultimate tensile strength (R_m), increases with increasing rolling reduction, while elongation to fracture (A) and reduction of area (Z) decrease, but they still remain at a satisfactory level. Compared with hot-rolled specimen, strength of HR + ST 14 mm specimen is a little smaller, but its impact toughness at −40 °C is the highest of 152 J. And the HRST14 exhibits a higher strength level than classical austenitic stainless steels. This excess in strength can be attributed to several factors, such as chemical composition, the grain size, and the interstitial nitrogen.

It was reported that the presence of nitrides and/or carbonitrides were detrimental to toughness, due to the grain boundary precipitates and ruptured mainly along grain boundaries [15–17]. Chandra Holm et al. [16] attributed the reduced fracture toughness to the $M_{23}(C, N)_6$ precipitates in cold worked samples formed during aging at temperatures between 600 and 900 °C. In this study, the final rolling pass is at 850 °C, and therefore precipitation happens preferentially along the grain boundaries. Although the toughness of hot-rolled plates at −40 °C is very low (Table 2), by comparison it can be found that the toughness of 10 mm plate is 29% higher than the 20 mm's, so it can be concluded that precipitates in the shape of warm-like along the grain boundary are even more detrimental. Mechanical properties obtained in tensile test are determined by final microstructural characterization. Due to lack of phase transformation and precipitation hardening, grain refinement and substructure can be used to greatly enhance the strength level. And at the same time during rolling process grain boundary precipitation should be avoided to ensure the toughnesss.

The product of strength and elongation ($R_m \times A$) is an important parameter for structural materials which represents the energy absorption capacity. The relationship between tensile strength and elongation to fracture is plotted in Fig. 5. In this figure, properties of samples cut along longitudinal direction of the plates are also listed here to present the overall performance. It shows that with the increase of R_m, the value of $R_m \times A$ decreases. It is worthy to be noted that the $R_m \times A$ of HRST14 HNS is the highest, which can approach 50 GPa%.

Examination of fracture surface

The fractographs of impact specimens are given in Fig. 6. Intergranular brittle fracture is the predominant failure mechanism for these two kinds of hot-rolled specimens, but they have some obvious differences. It can be noticed that fracture facets encircled by ridges of 10 mm plate are much smaller than those of the 20 mm plate, but their average grain sizes are almost the same (Fig. 1a, b). Such distinctness is caused by the carbides along the grain boundary (Fig. 2a, b), which can influence the crack propagation

Table 1 Characteristics of precipitation phases of hot-rolled plates

Sample name	Precipitation phase	Crystal system	Lattice parameter/nm	Phase structure	Wt%
HR2	$M_{23}C_6$	Fcc	$a_0 = 1.052–1.056$	$(Fe_{0.428}Cr_{0.572})_{23}C_6$	0.097
HR1	$M_{23}C_6$	Fcc	$a_0 = 1.060$	$(Fe_{0.448}Cr_{0.552})_{23}C_6$	0.109
	$(CrFe)_2N_{1-X}$ (trace)	Hexagonal	$a_0 = 0.4800$; $c_0 = 0.4462$	–	–

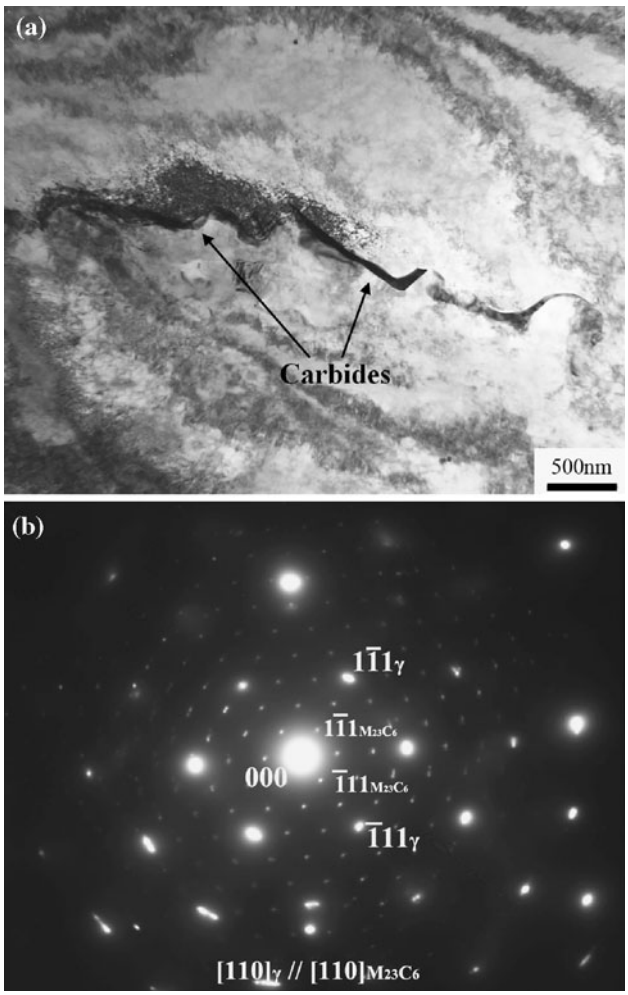

Fig. 4 TEM micrograph of carbides at grain boundary of HR2 plate **a** bright field images, long bars of carbides along grain boundary and **b** selected area electron diffraction pattern of precipitate, $[110]_\gamma$// $[110]_{M23C6}$

route. Coarse and continuous carbides along the grain boundary provide little resistance to the crack propagation, and crack cuts through this path quickly, finally leading to the complete failure of the specimen. And on the fracture surface coarse precipitates surrounding the grain can be spotted, as shown in Fig. 6b. The fracture of HRST14 sample has the characteristics of quasi-cleavage. The ST re-dissolves the carbides into the matrix and consequently strength of grain boundaries will be enhanced, which

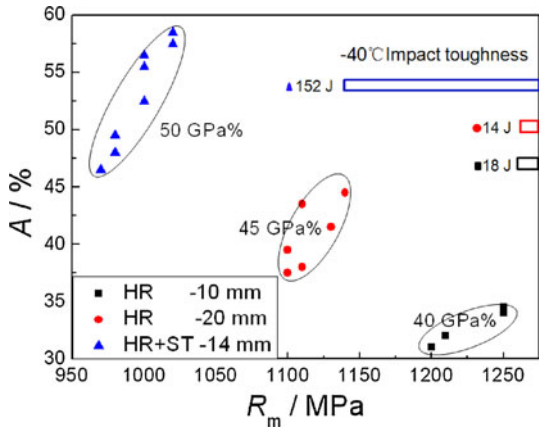

Fig. 5 Relationship between R_m and A for HNS at different processing states

means grain boundary is not the favorable route for crack propagation anymore. So higher impact absorption energy 156 J is achieved for the hot-rolled and solution-treated plate. There are annealing twins within cleavage facets and small amount of dimples along grain boundaries. Meanwhile, groups of slip lines with orientation relationship of 60° between them can be spotted (Fig. 6c).

Analysis of alloy composition and phases

A Schaeffler diagram can be used to predict the dependence of phase balance on chemical composition. And the nickel equivalent and chromium equivalent are used as the axes for the diagram, which are calculated by using the following expressions:

$$\text{Nieq} = \%\text{Ni} + \%\text{Co} + 0.1\%\text{Mn} - 0.01\%\text{Mn}^2 + 18\%\text{N} + 30\%\text{C} \quad (1)$$

$$\text{Creq} = \%\text{Cr} + 1.5\%\text{Mo} + 1.5\%\text{W} + 0.48\%\text{Si} + 2.3\%\text{V} + 1.75\%\text{Nb} + 2.5\%\text{Al}. \quad (2)$$

where all concentrations are expressed in weight percentage.

Calculated through these expressions, the two values of the material in this study are Nieq = 15.794 and Creq = 21.4, respectively. And it is just located in the full austenite phase zone, not far from the dividing line between

Table 2 Mechanical properties of the as-received materials with different processing conditions

Code name (strain %)	R_m/MPa	$R_{P0.2}$/MPa	A/%	Z/%	HRC	A_{KV} (−40 °C)/J
HR2-20 mm (88.9)	1110	870	39.5	61.5	33.7	14.0
HR1-10 mm (94.4)	1205	1035	31.5	55.5	41.1	18.0
HRST-14 mm (92.2)	980	645	48.5	70.5	25.8	152

R_m tensile strength; $R_{p0.2}$ yield strength; A elongation to fracture; Z area reduction; *HRC* Rockwell hardness; A_{KV} V-notch impact toughness

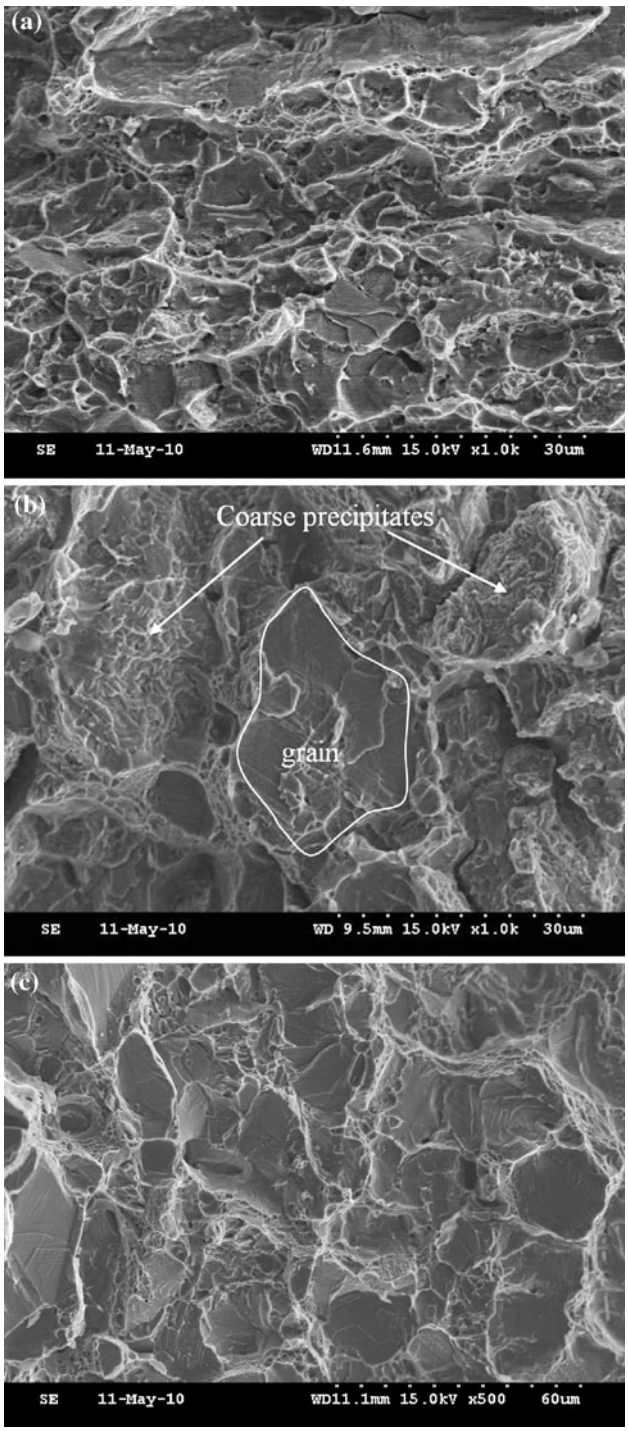

Fig. 6 SEM morphology of fracture surface at −40 °C **a** HR1, $A_{kv} = 18$ J; **b** HR2, $A_{kv} = 14$ J, coarse precipitates surrounding the grain; and **c** HRST14, $A_{kv} = 156$ J, quasi-cleavage fracture

austenite and ferrite, as shown in Fig. 7. However, during the solidification process of continuous casting, with the concentration increase of ferrite forming elements driven by pro-solidified austenites, small amount of ferrite will appear in the center of the slab along the direction of thickness. This kind of ferrite formed at high temperatures

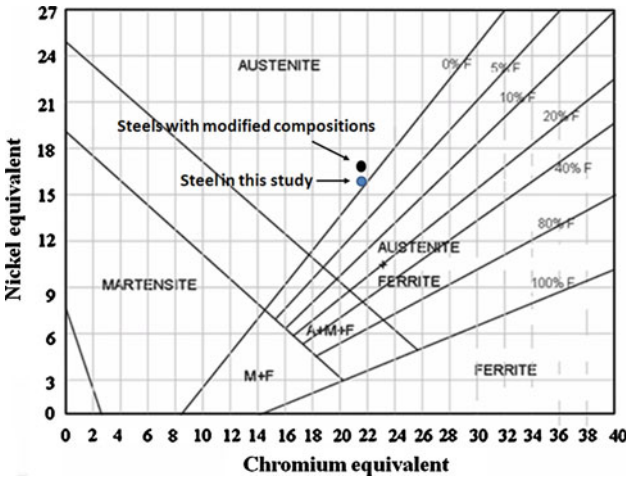

Fig. 7 Schaeffler constitution diagram for stainless steels

will exist all through the process of reheatment before hot rolling (Fig. 1c) and ST (Fig. 1d). Two simple methods can be applied to avoid ferrites by increasing the content of nickel or nitrogen, which leads to the increase of Nieq and unchanged Creq. But attentions should be paid to the solubility of nitrogen in the stainless steel and its decrease caused by increased Ni content.

Equation 3 depicts the correlation between solubility of nitrogen in weight percent and element content for practical purposes [18]. In this equation, nitrogen partial pressure is fixed to one atmosphere (or slightly below) and the temperature range under consideration is 1460–1500 °C (this being close to the lower end of the temperature range of AOD applied in this study). This equation also tells us the addition of Cr can effectively increase the solubility of N. Therefore, although it is possible to obtain full austenitic structure by adding less Cr, the simultaneously reduced N content will result in decreased strength, so this method is not adopted here.

$$\%\mathrm{N} = 0.067\%\mathrm{Cr} + 0.02\%\mathrm{Mn} + 0.04\%\mathrm{Mo} - 0.01\%\mathrm{Ni} - 1.0. \quad (3)$$

By using this equation it can be calculated that the %N in the material studied in this study is 0.732 wt%, so higher nitrogen content can be achieved. When the content reaches 0.71%, the value of Nieq will be increased to 16.874. When the content of Ni is added to 3.0%, the value of Nieq will be 16.949 with the solubility of nitrogen decreased to 0.715%. And the steels with modified compositions are also shown in Fig. 7.

Conclusions

The microstructures and mechanical properties of a HNS steel (0.65N–1.8Ni) manufactured by AOD and

continuous casting followed by different processing of HR (hot rolling) or HR and ST were studied in this article. The plate with the highest deformation stain has the highest strength. 50 GPa% (tensile strength × elongation to fracture) at room temperature and 152 J of impact toughness at −40 °C were achieved for the HR + ST plate. The toughness of hot-rolled plates is much smaller, in which $M_{23}C_6$ ($[110]_\gamma//[110]_{M23C6}$) is the main precipitate. The worm-like carbides formed during the finish forgings at 850 °C along grain boundary, at which crack propagates easily, are important reason causing deteriorated toughness. Intergranular brittle fracture is the predominant failure mechanism for hot-rolled specimens, while as for HR + ST ones the fracture surface has the characteristics of quasi-cleavage. There exists trace amount of ferrites caused by element segregation during solidification process in the as-received steels, to ensure full austenitic structure, composition modification, i.e., increased Nieq with unchanged Creq, can be adopted.

Acknowledgements The authors would like to thank professor Fan Rong and senior engineer Yu-ping Lang for helpful discussions.

References

1. Müllner P, Solenthaler C, Uggowitzer P, Speidel MO (1993) Mater Sci Eng A 164(1–2):164
2. Lee TH, Oh CS, Kim SJ (2008) Scripta Mater 58:110
3. Schino AD, Kenny JM (2003) Mater Lett 57:1830
4. Lach E, Anderson C, Schirm V, Koerber G (2008) Int J Impact Eng 35:1625
5. Singh BB, Sivakumar K, Bhat TB (2009) Int J Impact Eng 36:611
6. Lach E, Koerber G, Scharf M, Bohmann A (1999) Int J Impact Eng 23:509
7. Chen R, Shi J, Dong H, Liu YL, Gu YL, Rong F (2006) Ordnance Mater Sci Eng 29(2):46
8. Ikegami Y, Nemoto R (1996) ISIJ Int 36(7):855
9. Li HH, Jiang ZH, Cao Y, Zhang ZR (2009) Int J Miner Metall Mater 16(4):387
10. Balachandran G, Bhatia ML, Ballal NB, Rao PK (2000) ISIJ Int 40(5):478
11. Balachandran G, Bhatia ML, Ballal NB, Rao PK (2000) ISIJ Int 40(5):491
12. Simmons JW, Covino BS Jr, Hawk JA, Dunning JS (1996) ISIJ Int 36(7):846
13. Kim YS, Nam SM, Kim SJ (2007) J Mater Process Technol 187–188:575
14. Koutský J, Nový Z (1998) J Mater Process Technol 78:112
15. Simmons JW (1995) Scripta Metall 32(2):265
16. Holm HC, Uggowitzer PJ, Speidel MO (1987) Scripta Metall 21(4):513
17. Mathew MD, Sasikala G, Bhanu Sankara Rao K, Mannan SL (1991) Mater Sci Eng A 148(2):253
18. Speidel MO, Speidel HJ (2006) Proceedings of international conference on high nitrogen steels. Jiuzhaigou, China, 21–29